Thermally Tunable Metallodielectric Photonic Crystals from the Self-Assembly of Brush Block Copolymers and Gold Nanoparticles

*Dong-Po Song, Cheng Li, Nicholas S. Colella, Xuemin Lu, Jae-Hwang Lee, and James J. Watkins**

Photonic crystals (PhCs) prepared via the self-assembly of block copolymers (BCPs) offer new opportunities for simple fabrication of flexible photonic devices or coatings in an inexpensive and scalable manner.[1] The microphase separation of BCPs into periodic lamellar, cylindrical, bicontinuous, and spherical morphologies is promising for building nanostructured 1D, 2D, and 3D PhCs that have diverse potential applications such as optical filters, reflectors, sensors, and optical cavities.[2–8] The precise control and selective incorporation of inorganic nanoparticles (NPs) into specific domains of the microphase-separated BCPs can be used to tune the optical constant of the target domains and create hybrid materials with unique optical properties.[9]

1D PhCs fabricated from periodic layered metallodielectric nanocomposites have a number of potential applications, both as simple reflectors as well as optical metamaterials for subwavelength imaging and the enhancement of nonlinear optics.[10] Until now, these nanocomposites have been created via sophisticated physical and chemical deposition methods including sputtering;[10] the rapid, scalable, and solution-based fabrication of metallodielectric 1D PhCs based on self-assembly, including the application of linear BCPs, remained challenging due to the slow kinetics of the self-assembly process, the poor alignment of the lamellar structure, and the limited loading of metal additives such as noble NPs within well-ordered nanocomposites. Moreover, the domain size of the nanocomposites based on the self-assembly of linear BCP is typically a few tens of nanometers which is not large enough to open a photonic band gap (PBG) for visible light.[11–18] More than a decade ago, the Thomas group demonstrated an example of metallodielectric PhCs containing polystyrene-coated gold NPs to enhance the refractive index contrast and reflectivity.[9a,b] However, the low loading of the metal NP cores (<5 wt%) limits the utility of this system for the fabrication of metamaterials that have useful metallic photonic behaviors such as strong localized surface plasmon resonance (LSPR), and the tuning range of its PBG was also limited (560–640 nm).

In this work, we demonstrate a simple strategy for rapid and scalable fabrication of well-ordered metallodielectric 1D PhCs using amphiphilic brush BCPs as the templates and H-bonding as a driving force for the selective incorporation of gold NPs into hydrophilic domains (see **Figure 1**). We express the concentrations of the gold NPs as the weight percentage (wt%) of the nanocomposites based on the mass of the NP core and ligand shell, while the wt% of the NP core (Au%) was determined using the thermogravimetric analysis (TGA) of the composite and reflects the Au metal content of the composite. The content of the gold NPs of ≈2 nm in a core diameter was up to 67.2 wt% (Au% = 48.4 wt%), corresponding to 80.4 wt% of the gold NPs (Au% = 58.1 wt%) in the hydrophilic domain. By varying the gold NP loading quantity or the molecular weight of the brush BCP, highly ordered metallodielectric structures with the domain spacing controlled from 120 to 260 nm were readily created resulting in widely tunable PBGs from the visible to near-IR region (458–1010 nm). Moreover, the PBG is also tunable via thermally induced ripening of the NPs, which influences their size as well as their distribution (see Figure 1). A network structure of gold NPs with diameters greater than 10 nm was formed after thermal annealing leading to greatly increased conductivity and higher effective refractive index of the gold NP layer. The optical properties of the metallodielectric PhCs were significantly influenced by the network structure of gold NPs, which is tunable simply through the variation of annealing time. Numerical modeling using transfer matrix methods was employed to quantify the optical characteristics influenced by the effective conductivity of the gold NP network and showed a good agreement with the experimental results.

Recently, chemists have made a significant progress in design and synthesis of brush BCPs which show substantially reduced polymer chain entanglements relative to their linear analogues. This enables rapid self-assembly to yield nanostructures with domain sizes on the order of several hundreds of nanometers.[19–25] Introducing metal NPs into the large microdomains of phase-separated brush BCPs is of great interest from both fundamental research and application viewpoints. In our work, the brush BCPs were well-defined (polynorbornene-*g*-polystyrene)-*b*-(polynorbornene-*g*-poly(ethylene oxide)) block copolymers ($(PNB\text{-}PS_{3.5k})_n$-*b*-$(PNB\text{-}PEO_{2k})_m$) synthesized by sequential ring opening metathesis polymerization (ROMP) (see the Supporting Information for details). The molecular weight of the

Dr. D.-P. Song, C. Li, N. S. Colella, Prof. J. J. Watkins
Department of Polymer Science and Engineering
University of Massachusetts Amherst
120 Governors Drive, Amherst, MA 01003, USA
E-mail: watkins@polysci.umass.edu
Prof. X. Lu
School of Chemistry and Chemical Engineering
Shanghai Jiao Tong University
800 Dongchuan Road, Shanghai 200240, P. R. China
Prof. J.-H. Lee
Department of Mechanical and Industrial Engineering
University of Massachusetts Amherst
160 Governors Drive, Amherst, MA 01003, USA

DOI: 10.1002/adom.201500116

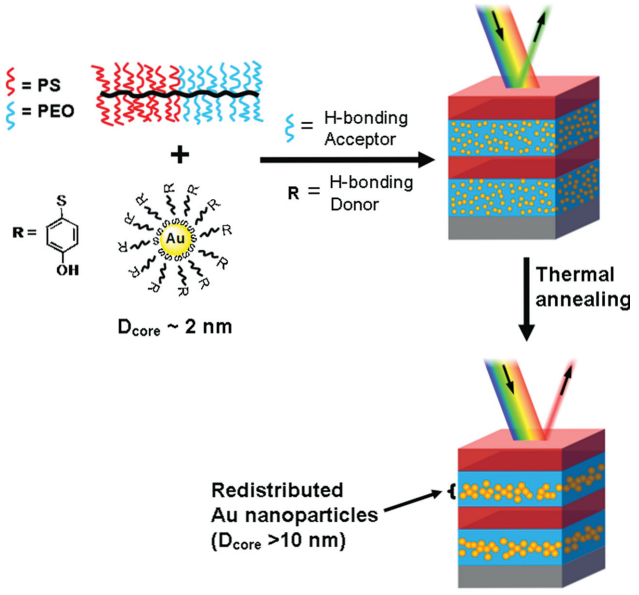

Figure 1. Illustration of the structure of metallodielectric 1D PhCs and the tuning mechanism via thermal annealing. The photonic films were prepared by self-assembly of PS-*b*-PEO brush BCPs and gold NPs around 2 nm in a core diameter. Variation of BCP molecular weight or gold NP loading modulates the domain spacing and/or refractive index contrast, and accordingly shifts the wavelengths of reflected light. Thermal annealing of the photonic films at 120 °C enhances the refractive index contrast and conductivity via increasing the size of gold NPs as well as the morphology of gold layers and results in a significant red shift of reflected light.

PS brush was 3.5 kg mol^{-1} (about 33 repeat units) while PEO brush had a molecular weight of 2 kg mol^{-1} (about 45 repeat units). The subscripts *n* and *m* represent the degree of polymerization (DP) of each block. Representative proton nuclear magnetic resonance (^{1}H NMR) spectra and gel permeation chromatography (GPC) traces can be found in Figures S1–S4 (Supporting Information). Molecular weight information for the polymer series has been summarized in Table S1 (Supporting Information).

Small-angle X-ray scattering (SAXS) was used to determine the bulk morphology of these brush BCPs. The PS-*b*-PEO bottle brushes self-assembled into well-ordered lamellar morphologies as indicated by the SAXS spectra (Figure S5, Supporting Information). A systematic shift in the location of the scattering vector of the first-order peak and higher-order peaks was observed with increasing molecular weight, indicating that the domain spacing increased from 44 to 185 nm. Transmission electron microscopy (TEM) was also used to verify the lamellar morphology, and TEM images (see Figure S6 in the Supporting Information) of the stained samples further confirmed the well-ordered lamellar morphologies, consistent with the SAXS data.

Four different brush BCPs (PNB-PS$_{3.5k}$)$_n$-*b*-(PNB-PEO$_{2k}$)$_m$ (**E**, n = 127, m = 221; **F**, n = 142, m = 248; **G**, n = 177, m = 264; **H**, n = 190, m = 332) were chosen for fabrication of the 1D PhCs. Gold NPs of ≈2 nm in a core diameter were prepared according to the literature procedures with 4-mercaptophenol ligands (see TEM image in Figure S7 in the Supporting Information).[15] The ligand was not only a stabilizer for gold NPs but also a hydrogen donor that exhibited strong H-bond interactions with the PEO side chains of the brush BCP. The strong H-bond interaction enabled the selective incorporation and the high loading of the gold NPs into PEO domains as illustrated by Figure 1. For the brush BCP-NP composites, we typically prepared a 1.2% (w/v) polymer solution in anhydrous tetrahydrofuran (THF) admixed with various amounts of gold NPs, resulting in different weight percentages in the solid.

Briefly, the composite films were prepared simply by drop casting the solutions on horizontal glass substrates. The solution cast on glass was covered with a glass Petri dish, and the solvent was evaporated over 4 h under nitrogen atmosphere. After solvent evaporation, the resulting films were put under vacuum at a room temperature for 24 h to completely remove the solvent (see the Experimental Section for detailed description). By varying the NP loading amount or the molecular weight of the brush BCP, six metallodielectric PhC films with different colors were obtained as shown in **Figure 2**a. The four films from the left showing gradual color changes from blue to red were prepared from blends of brush BCP **F** (M_n = 995 kg mol^{-1}) with gold NPs at varying loading amounts, 39.6, 51.3, 58.3, and 67.2 wt%, corresponding to the NP core contents (Au%) of 28.5, 36.9, 42.0, and 48.4 wt% based on TGA (see Figure S8 in the Supporting Information). The right two films containing 58.3 wt% of gold NPs were prepared from brush BCPs **G** (M_n = 1150 kg mol^{-1}) and **H** (M_n = 1330 kg mol^{-1}), respectively. The reflection (Figure 2b) of the BCP nanocomposites containing high loading of metal NPs suggest that the influence of optical absorption on reflection was minimized when the metal components are arranged in periodic arrays, which is consistent with the previous simulation and experimental results.[10,26]

The reflection measurements were performed on a fiber-optic spectrometer (F20, Filmetrics, Inc.) with a normal incident light or on a UV/vis/NIR spectrometer (LAMBDA 1050, PerkinElmer, Inc.) equipped with an "integrating sphere" diffuse reflectance accessory at an incident angle of 8°. Reflection spectra obtained by the fiber-optic spectrometer (Figure S9, Supporting Information) and by the UV/vis/NIR spectrometer (Figure 2b) confirmed the large differences in peak reflection (λ_{max}) between these samples. A substantial red shift from the visible to near-IR (457–1010 nm) was observed with the increased loading of the gold NPs or the molecular weight of the brush BCP. The red shift (Figure 2c) of λ_{max} with the increasing gold content was due to the increase of both the domain size (d) and the refractive index (n) of NP/PEO layer according to Equation (1)[27]

$$\lambda_{max} = 2(n_1 d_1 + n_2 d_2) \quad (1)$$

Transfer matrix simulations were employed to rationalize the proposed mechanism (see the Supporting Information). The domain sizes of the PS and NP/PEO layers were estimated from analysis of cross-sectional scanning electron microscopy (SEM) images. As shown in Figure 2c, a highly linear trend (R^2 = 0.99) in increasing domain spacing as a function of increasing percentage of gold NPs was observed. The refractive indices of the NP/PEO layer were calculated using the known wavelengths of λ_{max}, layer thicknesses, and refractive index of the PS layer.

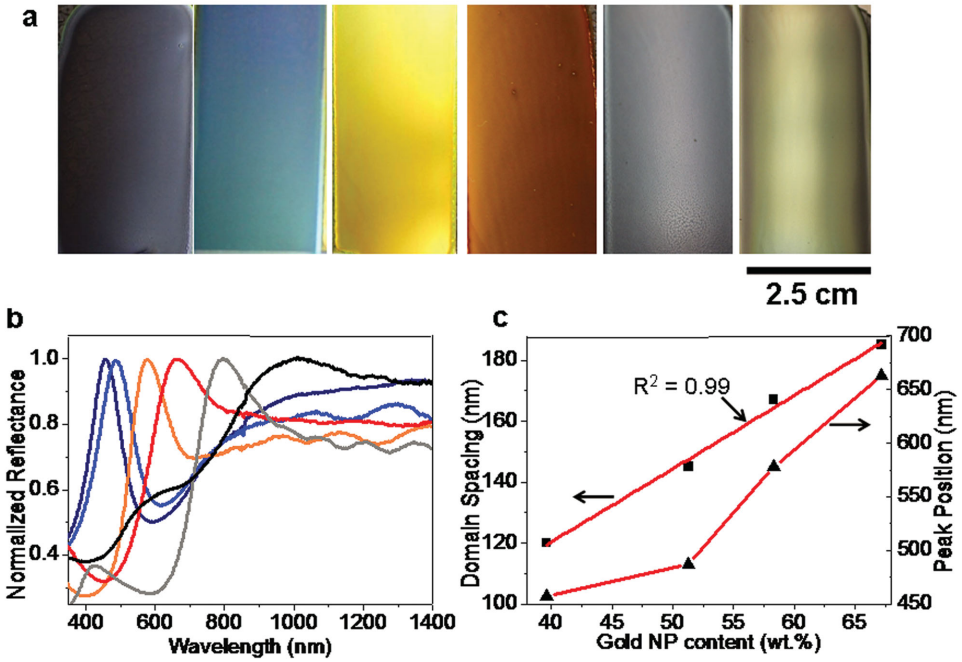

Figure 2. a) Photographs of composite films formed by self-assembly of PS-*b*-PEO brush BCPs and gold NPs showing tunable colors. The photographs were taken on a black background under fluorescent light. b) Normalized reflection from the films as a function of wavelength. c) The change of domain spacing and reflection peak position as a function of gold NP content. The domain spacings were estimated according to cross-sectional FESEM of the films (see Figure **3**).

Figure S10 (Supporting Information) shows an increase of the refractive index of the NP/PEO layer with the increasing gold NP loading.[28] The reflection spectra of the composite films containing various loading percentages of gold NPs show good agreement between the simulated and measured spectra (Figure S11, Supporting Information). The refractive index of the NP/PEO layer with 72.3 wt% of gold NPs was also measured using variable angle spectroscopic ellipsometry (VASE) for a blend of homopolymer PEO containing the same amount of gold NPs. In Figure S12 (Supporting Information), the measured refractive index ($n = 1.83$) at $\lambda_{max} = 578$ nm was close to the calculated value ($n = 1.90$), indicating good agreement.

Due to the large amounts of metal NPs selectively incorporated within the PEO domains and the wide lattice spacing, cross-sectional imaging of the composite films was possible without additional staining (see **Figure 3**) using field emission scanning electron microscopy (FESEM). Figure 3a–d shows the representative cross-sectional FESEM images of the blends of brush BCP **F** with gold NPs at varying loading percentages from 39.6 to 67.2 wt%. As shown in Figure 3a, poorly aligned layers were observed at the bottom of the sample with a

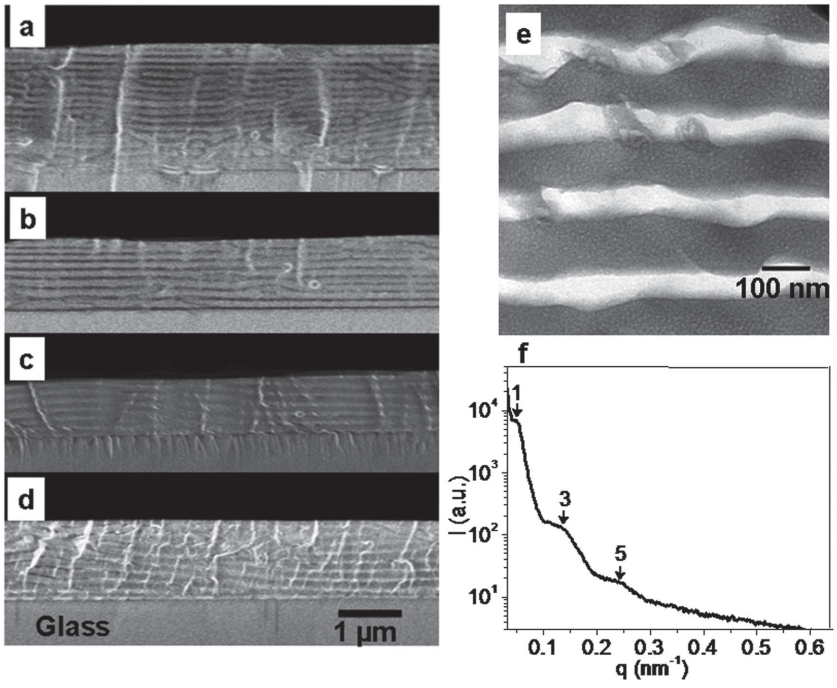

Figure 3. Characterization of the 1D PhCs formed from the blends of brush BCP **F** $(PNB\text{-}PS_{3.5k})_{142}$-*b*-$(PNB\text{-}PEO_{2k})_{248}$ with gold NPs. Cross-sectional FESEM images of the photonic films containing various loading amounts of gold NPs: (a) 39.6 wt.%; (b) 51.3 wt.%; (c) 58.3 wt.%; (d) 67.2 wt%. e) TEM image and f) SAXS profile confirm the well-ordered lamellar structure of composite sample (b). The film thicknesses of the different photonic films (a)–(d) are 1.9 μm, 1.1 μm, 932 nm, and 1.1 μm, respectively.

relatively low loading 39.6 wt%, while well-ordered structures with a general orientation of the layers parallel to the substrates were achieved at higher gold NP loadings up to 51.3 wt% (see Figure 3b–d). This can be explained by an additive-driven assembly mechanism: additives exhibiting strong H-bond interactions with specific domains can enhance the microphase segregation strength of BCPs and thus improve the morphology, consistent with our previous reports about linear BCPs.[15,29] Domain width is an important design parameter for our nanocomposites. By varying the loading percentage of gold NPs, the domain spacing was tuned from ≈120 (Figure 3a) to 185 nm (Figure 3d), the domain width of PEO/NP increased from 54 to 125 nm, and the PS domain decreased from 66 to 60 nm as measured using ImageJ. The significant swelling of PEO domain (131%) and slight contraction of the PS domain is consistent with selective confinement of the gold NPs within the PEO domain and strong segregation between the domains, even at very high NP loadings. A further increase of the domain spacing to 260 nm (Figure S13, Supporting Information) was achieved by brush BCPs with higher molecular weights (**G** and **H**). The well-ordered lamellar structure was further confirmed by TEM (Figure 3e) and SAXS (Figure 3f). We note that since PS and PEO of the unstained samples have similar electron densities, the contrast observed in the TEM image is evidently due to the gold NPs residing exclusively in PEO domains. The SAXS profile of the sample containing 51.3 wt% of gold NPs shows a primary scattering peak at $q = 0.045$ nm^{-1} indicating a phase separation of the BCP into a periodic nanostructure with a domain spacing of about 139 nm, consistent with the FESEM and TEM results. The well-ordered lamellar structure is confirmed by the higher-order reflections located at $3q$ and $5q$. To our knowledge, this is the first demonstration that brush BCPs can be used for assembly of inorganic NPs into nanostructured polymer hybrid materials with widely tunable lattice parameters and high filling fractions of NPs.

The distribution of NPs in microdomains of BCPs can be influenced by NP size according to both the reported simulation and experimental results, and large NPs tend to segregate to the center of the microdomains to alleviate polymer chain stretching penalties associated with accommodation of the large NPs while small NPs are more uniformly distributed.[9c,14] Thus, thermal annealing was performed on the metallodielectric 1D PhCs to increase NP size and investigate the annealing effects on their optical properties. Interestingly, a color change was evident after thermal annealing. **Figure 4**a shows the color change from yellow to red for the blend of brush BCP **F** with 58.3 wt% of the gold NPs after heating at 120 °C for 8 h. This is confirmed by a significant red shift of the peak reflection from 598 to 736 nm as indicated by Figure 4b. The TEM images provided insight into the annealing effects on NP size, distribution, and the morphology. TEM image analysis indicates an increase of the NP size and localization of the gold NPs to the center region of the

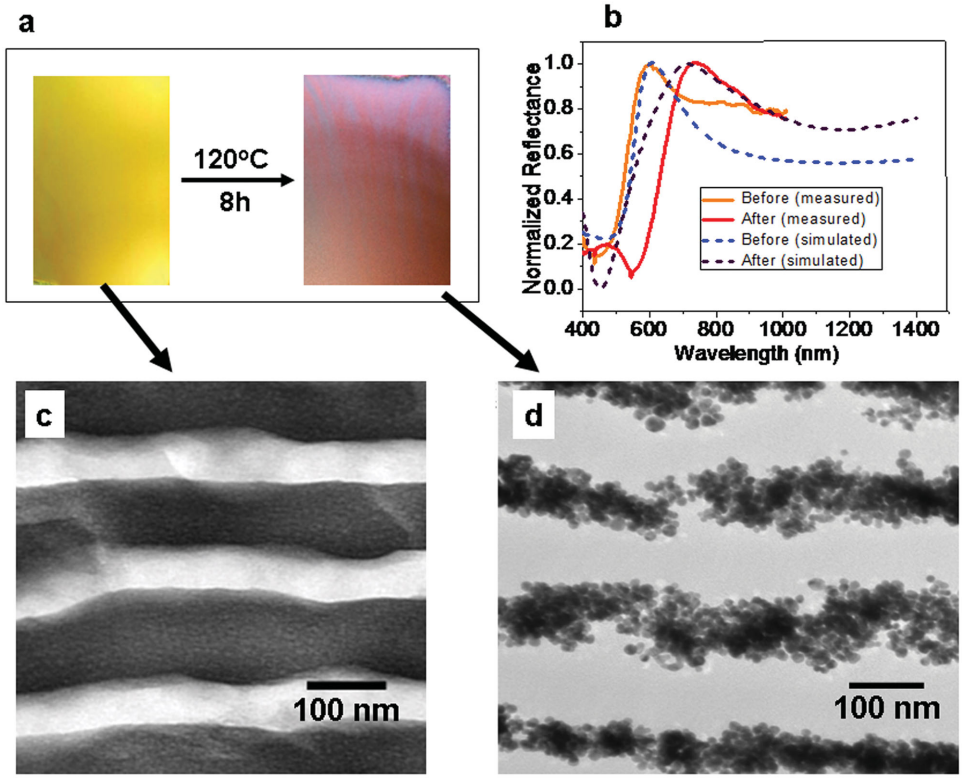

Figure 4. Illustration of a color change induced by thermal annealing. The sample is a blend of brush BCP **F** (PNB-PS$_{3.5k}$)$_{142}$-*b*-(PNB-PEO$_{2k}$)$_{248}$ with 58.3 wt% of gold NPs, and the thermal annealing was performed at 120 °C under vacuum for 8 h. a) Photographs of the film before and after thermal annealing. The photographs were taken on a black background under fluorescent light. b) The reflection of the film before and after thermal annealing shows good agreement between the simulated (dashed) and measured (solid) spectra. c,d) TEM images of the film before and after thermal annealing, showing the increased NP size and the redistribution of gold NPs in a layered structure.

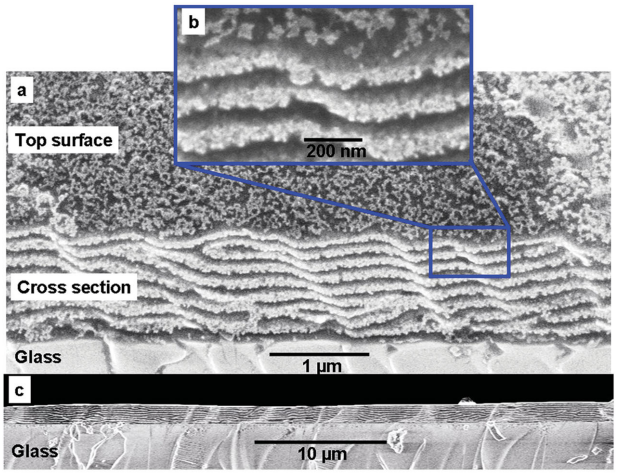

Figure 5. Cross-sectional FESEM images of the annealed film in Figure 4, showing alternating metallodielectric layers and a network structure of gold NPs. a,b) The images at different magnifications were obtained at a view angle of 45°. The sample was exposed to oxygen plasma for 20 s, and the etching depth was about 40 nm. The sawtooth shape of the cross section was formed during sample preparation. c) The side view of the sample without etching.

PEO domain (Figure 4c,d) upon thermal annealing. Although the molecular backbone of the brush BCP is highly stretched because of the steric congestion of densely grafted polymer brushes, entropic considerations associated with stretching of the side chains as well as the backbone likely influences the distribution of gold NPs, in a similar manner to that of linear BCP based nanocomposites.[9c,14] The well-ordered brush BCP blend structure was further confirmed by FESEM images (**Figure 5**) of cross sections of the annealed sample with the gold NP layers appearing as bright regions. Figure 5a,b shows the SEM of the oxygen plasma etched sample, and a network structure of gold NPs within the PEO domains was exposed on the top surface of the sample. Figure 5c shows the long range order of the metallodielectric structure from side view.

Since no obvious change in domain spacing was observed after thermal annealing based on TEM analysis (Figure 4c,d), VASE was used to investigate annealing effects on the refractive index of the NP/PEO layer using the blend of PEO with 73.2% of gold NPs. The refractive indices in the wavelength range from 400 to 1500 nm were significantly increased after thermal annealing (Figure S12, Supporting Information), indicating the red shift of reflection (Figure 4b) is primarily controlled by an enhancement of the refractive index contrast between polymer and metal-containing layers (Figure 1). Transfer matrix simulations were employed to model the reflection spectra of the sample before and after thermal annealing to rationalize the proposed mechanism. Conductivity parameters were incorporated into the simulation, and the NP/PEO layer of the annealed sample was found to be about four times more conductive than the nonannealed one. In Figure 4b, the response to thermal annealing shows good agreement between experimental and simulated spectra. The higher reflectance for the longer wavelengths is a typical trend from a metallic PBG.[30] Similar to 3D metallic PhCs, light can be transmitted through the sparse network of gold NPs, and therefore the major peak of reflection was observed due to the 1D PBG along the direction perpendicular to the metallodielectric multilayered structure.

Simulations were also performed to further investigate how conductivity will influence the reflection of light for the 1D metallodielectric PhC (see Figure S14 in the Supporting Information). A decrease of the major reflection peak and an increase of the reflectance in the long wavelength regime were observed with the increasing conductivity, and the major peak was finally disappeared at a critical value of the conductivity. This is consistent with the experimental results of a sample after extended thermal annealing (Figure S15, Supporting Information). The enhancement of conductivity by thermal annealing is also suggested by the continuous gold network formed in some regions of the PEO domain (see TEM image in Figure S15 in the Supporting Information). Both our simulation and experimental results indicate that it is possible to tune the optical properties of our PhCs through the design of the network morphology of gold NPs by thermal annealing and the tuning of conductivity as well as the refractive index of the metallic layer.

To investigate the kinetics of thermal annealing effect on reflection, a series of reflection measurements was performed on a sample after several annealing times at a temperature of 120 °C. A red shift of the peak reflection was observed as a result of the thermal annealing (see **Figure 6**a), consistent with the phenomenon observed for the sample in Figure 4. Moreover, the reflectance in the longer wavelength range increases with the increase of annealing time, which is consistent with

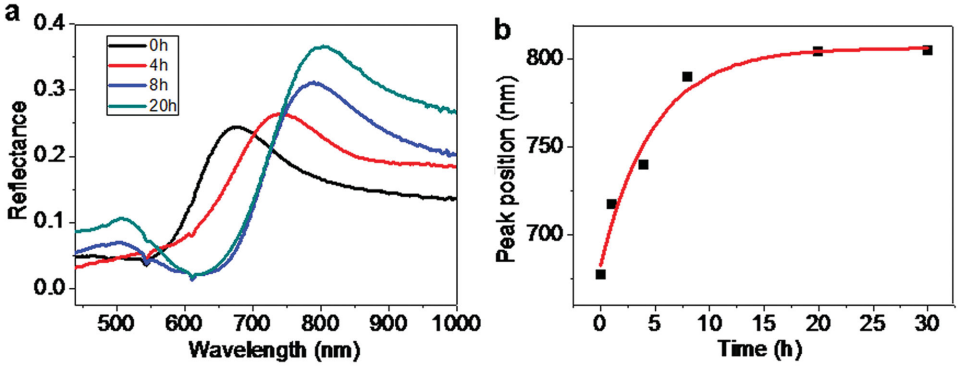

Figure 6. Thermal annealing effect on the reflection of a blend of brush BCP **E** (PNB-$PS_{3.5k}$)$_{127}$-*b*-(PNB-PEO_{2k})$_{221}$ with 67.2 wt% of gold NPs. a) Reflection from the blend as a function of wavelength. b) The change of reflection peak position as a function of annealing time.

our simulation results (Figure S14, Supporting Information). As seen in Figure 5b, the peak position (λ_{max}) is exponentially related to the annealing time (t) given by Equation (2)

$$\lambda_{max}(t) = \lambda_{max}(0) + \Delta\lambda_{max}(1 - e^{-t/\alpha}) \quad (2)$$

where λ_{max} (0) = 683 nm, $\Delta\lambda_{max}$ = 123 nm, and α = 4.88 h.

This provided a simple way to design the structure of the gold layer and to tune the optical properties of the PhCs through thermal annealing with a large tuning ratio, $\Delta\lambda_{max}/\lambda_{max}$ (0) approaching 20%. The ripening of NPs during thermal annealing was also monitored using the absorption spectrum of a film prepared by blade coating, and the absorption is due to the LSPR of the gold NPs.[31] The enhanced absorption and the red shift (see Figure S16, Supporting Information) of the peak position after thermal annealing indicate the increase of NP size.[31] The control over the NP size by thermal annealing enables the facile fabrication of well-ordered polymer nanocomposites with tunable plasmonic properties.

In summary, we present a robust strategy for rapid and scalable fabrication of metallodielectric 1D PhCs with high loading of metal NPs by using amphiphilic brush BCP as the template and hydrogen bonding as the driving force for domain-selective incorporation of the NPs. The lattice parameter of the periodic layered structure was precisely controlled from 120 to 260 nm by varying gold NP loading or molecular weight of the brush BCP. As a result, the reflection of light by the well-ordered structure is widely tunable from the visible to near-IR region. Moreover, the control over size as well as the distribution of the gold NPs in the well-ordered structure was realized through simple thermal treatment, showing significant effects on the photonic characteristics. This is primarily due to the greatly increased effective refractive index and conductivity of the gold NP layer as indicated by the simulation results through the creation of gold NP network in the PEO domain. This provides a way to precisely tune the optical properties of the metallodielectric PhCs through the design of the gold network structure simply by changing the annealing time. Similar to 3D metallic PhC, the novel metallodielectric PhC structure also allows light to pass through the gold NP layers as suggested by the major peak of reflection observed due to the constructive interference of light by the multilayered structure. In comparison with the nanocomposites based on linear BCPs, brush BCP provides a facile route to functional hybrid materials or devices with much higher loadings of functionalities and greatly expanded domain spacings. The simple processing and the rapid self-assembly of brush BCP nanocomposites make it promising to be used in roll-to-roll manufacturing.

Experimental Section

General Methods: *SAXS* measurements were performed using the SAXS instrument at Shanghai Synchrotron Radiation Facility (SSRF). The energy of incident X-ray was 12 keV and sample-to-detector distance was 7470 mm. Reflection measurements on the samples were performed on a PerkinElmer LAMBDA 1050 UV–vis–NIR spectrometer, equipped with a 150 mm integrating sphere diffuse reflectance accessory. All measurements were referenced to a spectralon reflectance standard with a 99% reflection. The light beam size was 7 mm in width and 15 mm in length. The reflection measurements were also performed on a fiber-optic spectrometer (F20 FILMETRICS) with a normal incident light. TEM measurements were conducted with a JEOL 2000FX TEM operated at accelerating voltages of 200 kV. Brush BCPs as well as the composites samples were embedded in epoxy and cured at room temperature overnight. Thin sections of ≈50 nm in thickness for microscopy were prepared using a Leica Ultracut UCT microtome equipped with a Leica EM FCS cryogenic sample chamber operated at −80 °C. FESEM measurements were carried out on a FEI Magellan 400 FESEM. The composites sample was cryofractured in liquid nitrogen to afford the cross sections for SEM.

Composite Sample Preparation: Appropriate amounts of brush block copolymers were weighed and dissolved in anhydrous THF followed by adding nanoparticle solutions in the same solvent to form about 1.2% (wt/v) stock solutions. The THF solutions were cast through 0.2 μm PTFE filters onto horizontal glass substrates which were covered immediately with glass Petri dishes, and the dried films after evaporation for about 4 h were put under vacuum at room temperature for about 24 h to completely remove residual solvent. We note that the evaporation of THF solutions was carried out under nitrogen atmosphere to control humidity below 20%. The composite sample of Figure 6 was prepared using a solution of a higher concentration of the mixture 4% (wt/v).

Supporting Information

Supporting Information is available from the Wiley Online Library or from the author.

Acknowledgements

The authors acknowledge the use of the Advanced Light Source, Shanghai Synchrotron Radiation Facility (SSRF). The authors thank Dr. Xiaohui Liu of their department for providing the 3rd generation Grubbs catalyst. The authors thank Rachel Letteri of their department for her help with the GPC measurements. This work was supported by the NSF Center for Hierarchical Manufacturing at the University of Massachusetts (CMMI-1025020).

Received: February 25, 2015
Revised: March 24, 2015
Published online: April 9, 2015

[1] a) Y. Fink, A. M. Urbas, M. G. Bawendi, J. D. Joannopoulos, E. L. Thomas, *J. Lightwave Technol.* **1999**, *17*, 1963; b) S. Valkama, H. Kosonen, J. Ruokolainen, T. Haatainen, M. Torkkeli, R. Serimaa, G. T. Brinke, O. Ikkala, *Nat. Mater.* **2004**, *3*, 872; c) Y. Kang, J. J. Walish, T. Gorishnyy, E. L. Thomas, *Nat. Mater.* **2007**, *6*, 957; d) J.-H. Lee, C. Y. Koh, J. P. Singer, S. Jeon, M. Maldovan, O. Stein, E. L. Thomas, *Adv. Mater.* **2014**, *26*, 532.

[2] a) F. S. Bates, M. A. Hillmyer, T. P. Lodge, C. M. Bates, K. T Delaney, G. H. Fredrickson, *Science* **2012**, *336*, 434; b) C. Park, J. Yoon, E. L. Thomas, *Polymer* **2003**, *44*, 6725.

[3] a) A. M. Urbas, S. Rachel, Y. Fink, E. L. Thomas, M. Xenidou, L. J. Fetters, *Adv. Mater.* **2000**, *12*, 812; b) T. Deng, C. Chen, C. Honeker, E. L. Thomas, *Polymer* **2003**, *44*, 6549; c) A. M. Urbas, M. Maldovan, P. De Rege, E. L. Thomas, *Adv. Mater.* **2002**, *14*, 1850; d) A. C. Edrington, A. M. Urbas, P. DeRege, C. X. Chen, T. M. Swager, N. Hadjichristidis, M. Xenidou, L. J. Fetters, J. D. Joannopoulos, Y. Fink, E. L. Thomas, *Adv. Mater.* **2001**, *13*, 421.

[4] A. M. Urbas, S. Rachel, Y. Fink, E. L. Thomas, M. Xenidou, L. J. Fetters, *Adv. Mater.* **2000**, *12*, 812.

[5] E. Kim, C. Kang, H. Baek, K. Hwang, D. Kwak, E. Lee, Y. Kang, E. L. Thomas, *Adv. Funct. Mater.* **2010**, *20*, 1728.
[6] a) H. S. Lim, J.-H. Lee, J. J. Walish, E. L. Thomas, *ACS Nano* **2012**, *6*, 8933; b) A. Noro, Y. Tomita, Y. Shinohara, Y. Sageshima, J. J. Walish, Y. Matsushita, E. L. Thomas, *Macromolecules* **2014**, *47*, 4103.
[7] C. Kang, E. Kim, H. Baek, K. Hwang, D. Kwak, Y. Kang, E. L. Thomas, *J. Am. Chem. Soc.* **2009**, *131*, 7538.
[8] a) J. Ge, Y. Yin, *Angew. Chem.* **2011**, *123*, 1530; J. Ge, Y. Yin, *Angew. Chem. Int. Ed.* **2011**, *50*, 1492; b) J. F. Galisteo-López, M. Ibisate, R. Sapienza, L. S. Froufe-Pérez, Á. Blanco, C. López, *Adv. Mater.* **2011**, *23*, 30; c) J. Wang, Y. Zhang, S. Wang, Y. Song, L. Jiang, *Acc. Chem. Res.* **2011**, *44*, 405; d) C. I. Aguirre, E. Reguera, A. Stein, *Adv. Funct. Mater.* **2010**, *20*, 2565; e) J. H. Moon, S. Yang, *Chem. Rev.* **2010**, *110*, 547.
[9] a) M. R. Bockstaller, R. Kolb, E. L. Thomas, *Adv. Mater.* **2001**, *13*, 1783; b) M. R. Bockstaller, E. L. Thomas, *J. Phys. Chem. B* **2003**, *107*, 10017; c) M. R. Bockstaller, Y. Lapetnikov, S. Margel, E. L. Thomas, *J. Am. Chem. Soc.* **2003**, *125*, 5276.
[10] a) A. Convertino, A. Capobianchib, A. Valentinic, E. N. M. Cirillo, *Adv. Mater.* **2003**, *15*, 1103; b) P. A. Belov, Y. Hao, *Phys. Rev. B* **2006**, *73*, 113110; c) N. N. Lepeshkin, A. Schweinsberg, G. Piredda, R. S. Bennink, R. W. Boyd, *Phys. Rev. Lett.* **2004**, *93*, 123902; d) S. Narayanan, J. Choi, L. Porter, M. R. Bockstaller, *ACS Appl. Mater. Interfaces* **2013**, *5*, 4093.
[11] See selected reviews: a) M. R. Bockstaller, R. A. Mickiewicz, E. L. Thomas, *Adv. Mater.* **2005**, *17*, 1331; b) M. C. Orilall, U. Wiesner, *Chem. Soc. Rev.* **2011**, *40*, 520; c) J. Kao, K. Thorkelsson, P. Bai, B. J. Rancatoreb, T. Xu, *Chem. Soc. Rev.* **2013**, *42*, 2654.
[12] J. J. Chiu, B. J. Kim, E. J. Kramer, D. J. Pine, *J. Am. Chem. Soc.* **2005**, *127*, 5036.
[13] Y. Lin, A. Boker, J. B. He, K. Sill, H. Q. Xiang, C. Abetz, X. F. Li, J. Wang, T. Emrick, S. Long, Q. Wang, A. Balazs, T. P. Russell, *Nature* **2005**, *434*, 55.
[14] a) R. B. Thompson, V. V. Ginzburg, M. W. Matsen, A. C. Balazs, *Science* **2001**, *292*, 2469; b) A. C. Balazs, T. Emrick, T. P. Russell, *Science* **2006**, *314*, 1107.
[15] Y. Lin, V. K. Daga, E. R. Anderson, S. P. Gido, J. J. Watkins, *J. Am. Chem. Soc.* **2011**, *133*, 6513.
[16] S. G. Jang, E. J. Kramer, C. J. Hawker, *J. Am. Chem. Soc.* **2011**, *133*, 16986.
[17] S. C. Warren, L. C. Messina, L. S. Slaughter, M. Kamperman, Q. Zhou, S. M. Gruner, F. J. DiSalvo, U. Wiesner, *Science* **2008**, *320*, 1748.
[18] Y. Zhao, K. Thorkelsson, A. J. Mastroianni, T. Schilling, J. M. Luther, B. J. Rancatore, K. Matsunaga, H. Jinnai, Y. Wu, D. Poulsen, J. M. J. Fréchet, A. P. Alivisatos, T. Xu, *Nat. Mater.* **2009**, *8*, 979.
[19] J. Rzayev, *Macromolecules* **2009**, *42*, 2135.
[20] Y. Xia, J. A. Kornfield, R. H. Grubbs, *Macromolecules* **2009**, *42*, 3761.
[21] Y. Xia, B. D. Olsen, J. A. Kornfield, R. H. Grubbs, *J. Am. Chem. Soc.* **2009**, *131*, 18525.
[22] W. Gu, J. Huh, S. W. Hong, B. R. Sveinbjornsson, C. Park, R. H. Grubbs, T. P. Russell, *ACS Nano* **2013**, *7*, 2551.
[23] B. R. Sveinbjörnssona, R. A. Weitekampa, G. M. Miyakea, Y. Xia, H. A. Atwaterb, R. H. Grubbs, *Proc. Natl. Acad. Sci. USA* **2012**, *109*, 14332.
[24] G. M. Miyake, V. A. Piunova, R. A. Weitekamp, R. H. Grubbs, *Angew. Chem. Int. Ed.* **2012**, *51*, 11246.
[25] V. A. Piunova, G. M. Miyake, C. S. Daeffler, R. A. Weitekamp, R. H. Grubbs, *J. Am. Chem. Soc.* **2013**, *135*, 15609.
[26] a) A. J. Ward, J. B. Pendry, W. J. Steward, *J. Phys.: Condens. Matter* **1995**, *7*, 2217; b) M. Scalora, M. Bloemer, *Appl. Phys. Lett.* **1998**, *72*, 1676; c) M. Scalora, A. S. Pethel, J. P. Dowling, C. M. Bowden, A. S. Manka, *J. Appl. Phys.* **1998**, *83*, 2377; d) Y.-H. Ye, G. Bader, V.-V. Truong, *Appl. Phys. Lett.* **2000**, *77*, 235.
[27] A. C. Edrington, A. M. Urbas, P. DeRege, C. X. Chen, T. M. Swager, N. Hadjichristidis, M. Xenidou, L. J. Fetters, J. D. Joannopoulos, Y. Fink, E. L. Thomas, *Adv. Mater.* **2001**, *13*, 421.
[28] S. Kubo, A. Diaz, Y. Tang, T. S. Mayer, I. C. Khoo, T. E. Mallouk, *Nano Lett.* **2007**, *7*, 3418.
[29] a) V. K. Daga, J. J. Watkins, *Macromolecules* **2010**, *43*, 9990; b) V. R. Tirumala, V. Daga, A. W. Bosse, A. Romang, J. Ilavsky, E. K. Lin, J. J. Watkins, *Macromolecules* **2008**, *41*, 7978; c) V. R. Tirumala, A. Romang, S. Agarwal, E. K. Lin, J. J. Watkins, *Adv. Mater.* **2008**, *20*, 1603.
[30] J.-H. Lee, C. H. Kim, Y. S. Kim, K. M. Ho, *Appl. Phys. Lett.* **2006**, *88*, 181112.
[31] a) S. Link, M. A. El-Sayed, *J. Phys. Chem. B* **1999**, *103*, 8410; b) M. R. Jones, K. D. Osberg, R. J. Macfarlane, M. R. Langille, C. A. Mirkin, *Chem. Rev.* **2011**, *111*, 3736; c) J. A. Fan, C. Wu, K. Bao, J. Bao, R. Bardhan, N. J. Halas, V. N. Manoharan, P. Nordlander, G. Shvets, F. Capasso, *Science* **2010**, *328*, 1135.